Journal of the Physical Society of Japan **92**, 024201 (2023)
https://doi.org/10.7566/JPSJ.92.024201

Comparison Study of MCNP6 and GEANT4 for Neutron Transportation and Detection in ^{3}He Long Counter

Pilsoo Lee* and Nam-Woo Kang

Korea Multi-purpose Accelerator Complex, Korea Atomic Energy Research Institute, Mirae-ro 181, Gyeongju-si, 38180, Republic of Korea

(Received February 7, 2022; accepted November 30, 2022; published online January 13, 2023)

A long counter is a commonly used device for neutron-flux measurements in a wide energy domain. Although its physical structure is well defined, device's response differs significantly depending on the nature of radiation fields. We investigated a ^{3}He long counter under well-defined radiation fields based on experiments and Monte Carlo simulations. The responses of the long counter were evaluated in MCNP6 and GEANT4 simulations for neutrons at energies between 10 keV and 20 MeV. The simulation results were validated with experimental data obtained with the spontaneous-fission neutron of ^{252}Cf and quasi mono-energetic neutrons between 0.2 and 1.5 MeV. The results showed that MCNP6 underestimated count rates, calculated from the pulse-height distribution of recoiled particles in the neutron-induced nuclear reaction in the ^{3}He volume, while neutron transportation seems equivalent in both simulation tools. For a given condition, GEANT4 reproduced the experimental values well, and GEANT4 results appeared to be more realistic for detector simulations in the energy range of interest.

1. Introduction

A long counter is a neutron-measurement device constructed based on slow-neutron detectors surrounded by moderating materials; it is known to have a flat response curve over a wide neutron-energy range from a few eV up to a few MeV.[1,2] Because of these advantages, several types of long counters have been used as reference neutron-flux monitors in neutron facilities.[3,4]

Although neutron flux is a physical quantity for which such a neutron-measurement device can be utilized, flux is not directly measurable but deduced from other measured quantities such as total counts of electric pulses or partial integral of pulse-height distributions obtained using radiation detectors. Therefore, evaluating neutron-detector sensitivity, which is a relation between the neutron flux and the response of devices in neutron fields, is a key issue in using long counters in various neutron fields. Because the characteristics of usable neutron sources practically limit experimental evaluation of the sensitivity, the sensitivity is generally investigated by means of Monte Carlo simulations.

In one previous study,[4] a ^{3}He long counter, which was built based on the Hanson and McKibben design,[5] was developed as a neutron fluence monitor at a neutron facility. The long counter was investigated with simulations and experiments in the standard neutron facility at JAEA. It was found that the experimental results were in agreement with the simulation results at 144, 250, and 565 keV.

In the present study, we investigate a long counter under well-defined neutron fields, including radioactive and accelerator-based mono-energetic neutron sources. At the same time, we estimate the responses of the real-world detector based on two well-known particle transportation tools, MCNP6 and GEANT4. For the given conditions, the measured and calculated results are compared, and the prediction accuracy of the simulation tools is discussed.

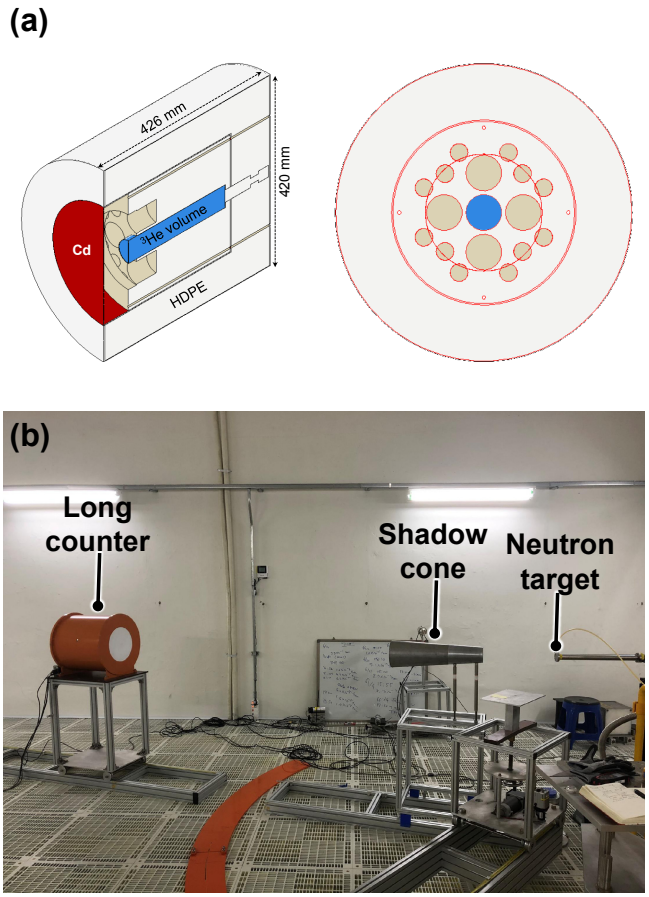

Fig. 1. (Color online) (a) Cross-sectional view of long counter at KOMAC and (b) experimental setup for neutron measurements with long counter and shadow cone. The shadow cone was used to evaluate the number of scattered neutrons in the environment by blocking the flight path of neutrons between the neutron target and the long counter. In the figure, the ^{3}He volume in the center of the long counter is depicted in blue.

2. Description of Long Counter

The ^{3}He long counter was initially built and used at the Korea Institute of Geoscience and Mineral Resources (KIGAM);[4] the counter was relocated to the Korea Multi-purpose Accelerator Complex (KOMAC) of the Korea Atomic Energy Research Institute (KAERI). A cross-sectional view of the long counter is shown in Fig. 1. The ^{3}He detector, having an active volume of 363.73 cm^3 in the long

counter, was filled with ^{3}He gas at 4 atm. The effective diameter and length of the ^{3}He tube were 4.77 and 20.32 cm.

A shadow cone, made of 198-mm-thick high-density polyethylene (HDPE) and 348-mm-thick iron encapsulated with a 1-mm-thick Cd sheet, was used to evaluate scattered neutrons. The long counter was built to count fast neutrons up to a few MeV, so the outside HDPE cylinder and Cd sheet were used to protect scattered neutrons from entering directly into the ^{3}He detector.[4)]

3. Monte Carlo Simulations

Neutron transportation through matter was simulated using Monte Carlo particle transport codes MCNP6[6)] and GEANT4.[7–9)] Versions of MCNP6 and GEANT4 were 6.2 and 10.6, respectively. The CAD geometries of the long counter were imported into the Monte Carlo simulations with the help of the external converting tools SuperMC[10,11)] for MCNP6 and CADMesh[12)] for GEANT4.

The following simulations adopted the same atomic compositions for HDPE (H:14.4 and C:85.6 in wt%) and air (C:0.01, N:75.5, O:23.19, and Ar:1.3 in wt%). For concrete, the atomic compositions tabulated in the reference[13)] and the NIST database were adopted for MCNP6 and GEANT4, respectively. It is worth noting that slightly different concretes produced almost identical results in separate simulations, and the scattered-neutron component can be eliminated based on the shadow-cone method.[14)]

In the ensuing Monte Carlo simulations, neutron transportation and the neutron-induced nuclear reaction ^{3}He(n,p)^{3}H were considered. The protons and tritons generated within the ^{3}He active volume were tallied; then, their energy-deposition spectra were analyzed as was also done for the experimental data. For a cross-section library in MCNP6, the default library, mostly comprised of ENDF/B-VII.1,[15)] in MCNP6.2 was invoked. On the other hand, for a library in GEANT4, the neutron high-precision models are based on JEFF-3.3.[16)] It is worth noting that ENDF/B-VII.1 and JEFF-3.3 have the same values for the ^{3}He(n,p)^{3}H reaction cross sections.

In the MCNP6 simulations, the neutron capture ion algorithm (NCIA) was invoked to produce recoiled particles in the neutron-induced reaction, and the pulse heights generated by the recoiled particles were scored using the F8 pulse-height tally, which is a new standard tally introduced in MCNP6. The thermal-neutron scattering kernel S(α,β) library for polyethylene was used for thermal-neutron scattering treatment.

High-precision models for neutron-interaction channels of elastic, inelastic, capture, and fission were employed to transport neutrons with kinetic energy below 20 MeV in GEANT4. The reference physics lists in GEANT4 that use high-precision models showed almost the same results for the neutron sources of interest. In GEANT4, prepackaged thermal-neutron scattering kernels were used to handle thermal neutrons. Here, we focused on neutron energy below 20 MeV, for which neutron transportation in both tools is based on data-driven physics models.

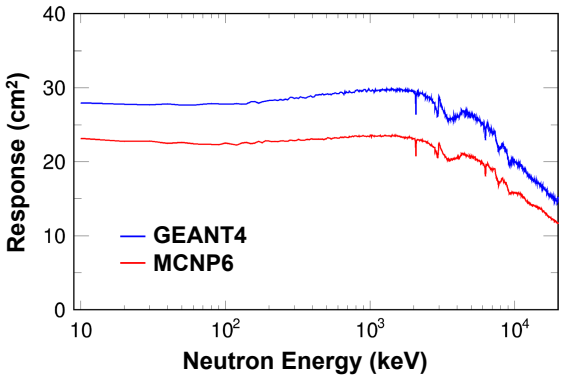

Fig. 2. (Color online) Simulated response functions of long counter for uniform and parallel neutron beams at energies between 10 keV and 20 MeV. Protons and tritons generated in ^{3}He(n,p)^{3}H reaction were scored in the simulations.

The simulations were carried out for three cases: intrinsic efficiency of long counter in a void exposed to mono-energetic neutrons, detector responses for ^{252}Cf source as function of distance between counter and source, and detector responses for quasi mono-energetic neutron beams produced by ^{7}Li(p,n)^{7}Be reaction.

In the first case, parallel mono-energetic neutron beams were uniformly generated on the front surface of the long counter at energies between 10 keV to 20 MeV in a step of 10 keV; intrinsic efficiency (or sensitivity), which was calculated by partial integration of pulse-height distribution divided by the number of incident neutrons on the detector surface, was obtained as shown in Fig. 2. Simulations were done only for the given geometries of the long counter in the vacuum space; therefore, the results do not include the in-scatter and out-scatter of neutrons by walls and the air. The results show that MCNP6 underestimated the intrinsic efficiency by an average of 21% compared to GEANT4. A large part of the difference between the tools came from the different algorithms used to calculate the recoiled-proton spectrum in the ^{3}He(n,p)^{3}H reaction. The calculated neutron cell flux of the tools shows an insignificant difference, as will also be presented for the other two cases. Differences between the tools will be revisited in the experiments, and in the analysis and discussion section.

For further investigation of the simulation models, a simplified experimental setup for neutron measurements was implemented to consider neutron scattering; then, simulation results were compared with corresponding experimental data.

In the second case, neutrons emitted via spontaneous fission of ^{252}Cf were generated with isotropic angular distribution and energy distribution defined by the Watt fission spectrum, whose mean energy corresponds to 2.14 MeV, as suggested in the MCNP6 user's manual. Lastly, neutrons in ^{7}Li(p,n)^{7}Be, for which the production cross-sections and angular distributions are well known at proton energies between 1.95 and 7.00 MeV,[17)] were generated at a LiF target disc. The kinetic energy of the neutrons emitted at scattering angle θ can be calculated according to the two-body energetics of the reaction:

$$E_n(E_p,\theta)^{1/2} = \frac{\cos\theta\sqrt{m_p m_n E_p} \pm \sqrt{m_p m_n E_p \cos^2\theta + (m_{Be}+m_n)[m_{Be}Q + (m_{Be}-m_p)E_p]}}{m_{Be}+m_n}, \quad (1)$$

where E_n and E_p are the kinetic energies of recoiled neutrons and incident protons, Q is the reaction Q value, and m_p, m_n, m_{Li}, and m_{Be} are the atomic masses of proton, neutron, ^{7}Li, and ^{7}Be, respectively.

4. Experiments, Analysis, and Discussion

Neutron measurements using the long counter with radioactive and quasi mono-energetic neutron sources were conducted at the neutron-target room for the quasi mono-energetic neutron source in the KOMAC of the KAERI.[18] The picture of the experimental setup in the room is provided in Fig. 1(b); the width, depth, and height of the room were $7.2 \times 8.7 \times 5.7$ m^3.

A series of conventional modules, composed of Canberra 2006 preamplifier, CAEN N968 spectroscopy amplifier, and CAEN N957 multichannel analyzer, was used for the signal processing and data acquisition of the long counter. The shaping time of the spectroscopy amplifier was 6 µs; the obtained spectra of the long counter are shown in Fig. 3(a).

4.1 ^{252}Cf source

For measurements with a radioactive neutron source, 85 µCi ^{252}Cf sealed in a 3036 capsule (ISO classification C66545) manufactured and calibrated by Eckert&Ziegler was used. The source was placed on the axis of the long counter; then, count rates were recorded at 5 different distances between 0.05 and 0.25 m at a step of 0.05 m. Below the plot of pulse-height distribution [Fig. 3(a)], simulated count rates along with experimental data points are presented in Fig. 3(b). The simulated count rates have a relative error of 3.1%, which comes from the uncertainty in the activity of ^{252}Cf used in the measurements; however this error is not drawn in the plots. It was found that GEANT4 reproduced experimental values well at each position, whereas MCNP6 underestimated count rates, as was also found in the intrinsic-efficiency case (Fig. 2). Relative differences between the results of MCNP6 and GEANT4 increased as distance increased, yielding an average deviation of 30%.

On the other hand, the relative difference between MCNP6 and GEANT4 of the neutron cell flux in the ^{3}He volume [Fig. 3(c)] were below 4% at 0.05, 0.10, 0.15, and 0.20 m and at around 8% at 0.25 m, respectively. As in the case of the intrinsic efficiency, MCNP6 underestimated count rates that were biased with respect to the GEANT4 results. It is worth noting that neutron scattering by air and walls was not considered in the calculation of intrinsic efficiency; therefore, scattered-neutron flux can introduce more deviation to the simulated count rates.

From a statistical point of view, the χ^2 test was selected as a goodness-of-fit test to quantitatively evaluate the equivalence between experimental data and simulation results in the ROOT framework:[19]

1) The null hypothesis stated the equivalence between experimental data and simulations for all proton energies

H_0: $F_{EXP}(E_p) = G_{SIM}(E_p)$

2) The alternative hypothesis stated that the simulated data differed for the proton energies

H_1: $F_{EXP}(E_p) \neq G_{SIM}(E_p)$.

The p-values of the test were found to be 0.999 and 0.968 for GEANT4 and MCNP6, respectively. At a confidence level $\alpha = 0.05$, the null hypothesis was accepted.

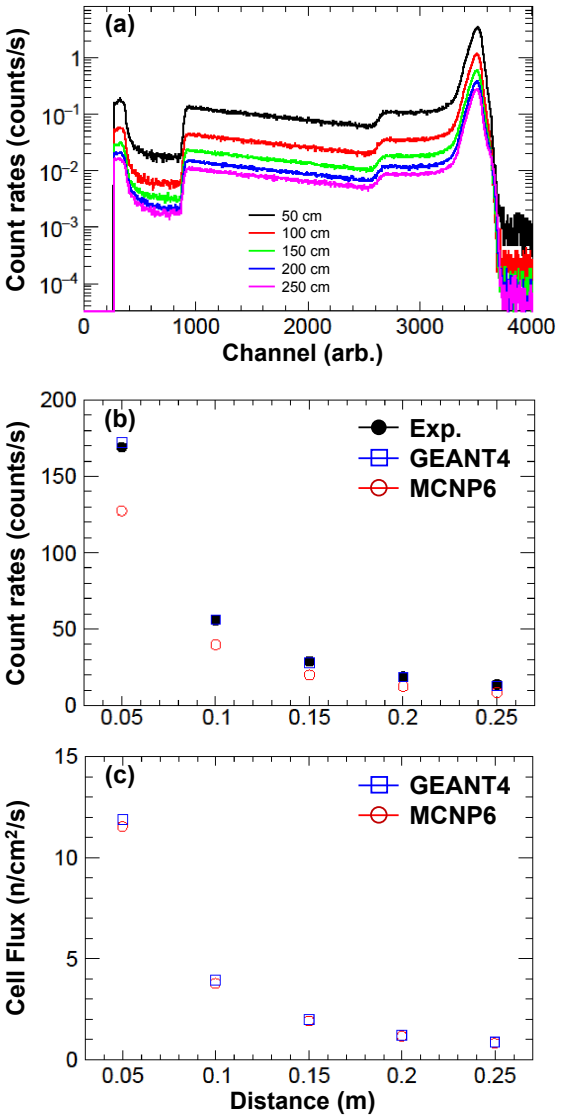

Fig. 3. (Color online) (a) Experimental spectra of long counter for 5 different source-detector distances against neutrons emitted in spontaneous fission of ^{252}Cf, (b) experimental and simulated count rates, and (c) simulated cell flux in ^{3}He active volume of long counter as function of distance between front surface of counter and source. In the figures, black (filled circles), red (empty circles), and blue (empty squares) markers indicate experimental values and MCNP6 and GEANT4 simulation results, respectively.

4.2 Quasi mono-energetic source

The neutron-production target was a LiF target, prepared by evaporating LiF powder on a thin Al substrate at a target thickness of 100 µg/cm^2; target was installed at the end of a proton beam line for neutron production.[18] The diameter of the target was 25 mm; the beam current was measured at the target.

During measurements with a quasi mono-energetic source, the long counter was fixed at 10° against the beam axis and 3 m away from the neutron target; the ^{3}He detector was placed at 0° for simultaneous energy measurements. The neutrons were measured at proton-beam energies between 2.0 and 3.0 MeV at a step of 0.1 MeV, corresponding to neutron energies between 222.9 and 1301.5 keV. For a given proton-beam energy (E_p), the neutron energy at 0° (E_n^0), measured full-width-at-half-maximum (FWHM), count rates of the long counter without and with a shadow cone, and deduced

Table I. Kinetic energy of injected proton beam (E_p), calculated neutron energy at 0° (E_n^0), measured FWHM of neutron beam at 0°, count rates at 10°, and sensitivity of long counter. The values in the square brackets are the scattered-neutron count rates measured with the shadow cone. See text for details.

E_p (MeV)	E_n^0 (keV)	FWHM (%)	Count rates (counts/uA)	Sensitivity (counts/n)
2.0	222.9	3.2	217.6 [53.6]	0.022
2.1	343.5	3.6	168.6 [60.5]	0.020
2.2	457.1	3.5	321.4 [88.8]	0.014
2.3	567.1	3.3	611.2 [114.0]	0.017
2.4	674.9	3.0	474.3 [53.4]	0.021
2.5	781.3	2.6	353.5 [60.3]	0.019
2.6	886.6	2.7	314.9 [27.4]	0.022
2.7	991.1	2.8	270.7 [57.1]	0.019
2.8	1095.0	2.4	261.3 [39.8]	0.021
2.9	1198.4	2.7	261.7 [57.2]	0.020
3.0	1301.5	2.2	253.3 [61.9]	0.020

sensitivity are given in Table I. The FWHM values at each neutron zero-degree energy were measured based on the ^{3}He(n,p) reaction with the ^{3}He detector.[20] The count rates were normalized with respect to the proton-beam current injected into the neutron target. The relative error in the measured count rates was 10%; this arose from proton-beam current measurements using a Faraday cup during neutron irradiation. Detector sensitivity was calculated based on the count rates measured without and with a shadow cone and the calculated number of mono-energetic neutrons on the front surface of the long counter. The number of neutrons on the detector surface was calculated using the cross-sections of the ^{7}Li(p,n) reaction.[17,18] The shadow-cone method[14] allows direct assessments of neutrons scattered from the air and wall; the scattered-neutron counts subtracted from the neutron count rates correspond to the neutron flux coming directly from the source. The shadow cone was placed along the flight path of neutrons from the neutron-production target to the detector, at a distance 400 mm away from the front surface of the target so it could completely block the path. The relative error in the sensitivity was estimated to be 14%, considering the relative error in the count rates. Plots of the measured count rates and corresponding simulation results are shown in Fig. 4.

As in the radioactive-source case, MCNP6 underestimated the experimental count rates with an average deviation of 32%, whereas the average deviation of GEANT4 was 1%. GEANT4 seems to overestimate the count rates at $E_p =$ 2.2 MeV. However, the count rates were lower than expected for unidentified reasons considering that the experimental sensitivity suddenly dropped at the proton energy 2.2 MeV.

The disagreement between experimental and simulated values at $E_p = 2.2$ MeV could be explained as the results of either (1) neutron-production deficit at $E_p = 2.2$ MeV or (2) neutron loss at $E_n = 457.1$ keV. The first hypothesis implies that there might be an error in the calculated neutron production rate. It is worth noting that the long counter was tilted against the beam axis, and the neutron-production rate at the tilting angle was calculated using Legendre polynomials based on the zero-degree differential cross-section and Legendre coefficients given in the review.[17] If the cross-section at the energy and angle deviated from the actual value, this would contribute to the observed discrepancy.

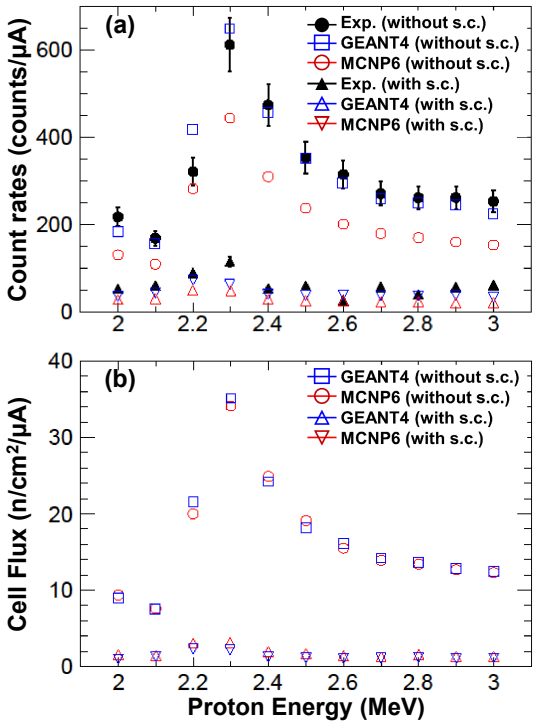

Fig. 4. (Color online) (a) Count rates and (b) simulated cell flux of long counter exposed to quasi mono-energetic neutron beams as function of proton-beam energies, E_p, injected to neutron production target. Black filled circles indicate experimental values, while blue and red markers show GEANT4 and MCNP6 simulation results. In the figures, squares and circles are measured and simulated values without shadow cone, while up- and down-pointing triangles are measured and simulated values with shadow cone. In the legend, *s.c.* means the shadow cone.

There have been few experimental studies of the ^{7}Li(p,n) reaction in the energy domain; further studies are strongly required to evaluate the uncertainty of the proton energy.

On the other hand, the second hypothesis raises the possibility of neutron loss in the measurements. Here we do not consider that the cross-section of ^{3}He(n,p) has a neutron-transparent window at $E_n = 457.1$ keV because the excitation function is a well-known smooth function in the energy domain; also the literature does not provide any experimental clues for this window.[15,16] Although it is unlikely that there were unidentified neutron absorbers with narrow resonances around this energy, there is currently no explanation for the neutron loss in the measurements.

The distributions were compared using χ^2 tests, and it was found in the normalized residuals that the values at $E_p =$ 2.2 MeV significantly influenced the GEANT4 and MCNP6 χ^2 results. Values were identified as outliers based on normalized residuals greater than 3. Excluding the outliers, the p-values were found to be 0.713 and 0.871 for GEANT4 and MCNP6, respectively; again, the hypothesis of identity was accepted at a confidence level of 0.05. Regarding the cell flux in the ^{3}He volume of the long counter, MCNP6 and GEANT4 showed minor deviations over the energy range of interest. To understand the origin of the deviations, the energy spectra of neutrons arriving at the ^{3}He tube of the long counter for proton energies in the range of $2.0 \leq E_p \leq$ 3.0 MeV were investigated, with results shown in Fig. 5. For the energy binning, the neutron energy group structure in one reference paper[21] was adopted. The energy spectra in

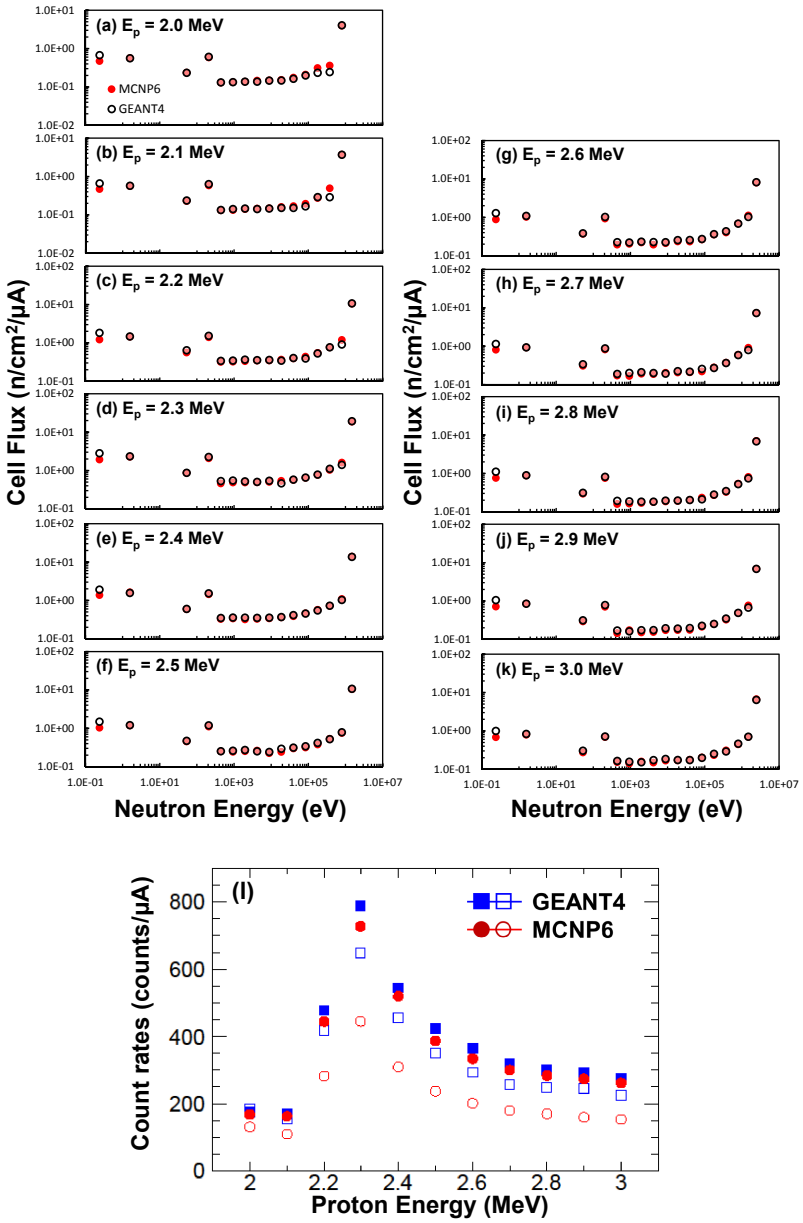

Fig. 5. (Color online) (a)–(k) Energy spectra of neutrons arriving at ^{3}He tube of long counter exposed to quasi mono-energetic neutrons for proton energies between $E_p = 2.0$ and 3.0 MeV. And (l) count rates calculated by (filled markers) multiplying neutron cell flux by the cross section at the mean energy of the ith bin and (empty markers) counting protons and tritons generated in the ^{3}He(n,p)^{3}H reaction.

Figs. 5(a)–5(k) show that MCNP6 and GEANT4 estimate almost identical energy spectra of neutrons reaching the ^{3}He volume, except for the first energy bin ($0.064 \leq E_n < 0.4$ eV). It is suspected that MCNP6 and GEANT4 have different thermalization processes, and the observed deviations can be attributed to the different neutron cell fluxes in the thermal-energy domain. Count rates were obtained by multiplying the neutron cell flux by the cross-section at the mean energy of the ith bin [Fig. 5(l)]. In the energy domain, all GEANT4 values are larger than MCNP6 values because of cell-flux differences; however, the differences are not as significant as the deviations observed in the simulated count rates shown in Fig. 4. The count rates based on cell-flux calculations show that deviations between count rates obtained in MCNP6 and GEANT4 by counting protons and tritons generated in the ^{3}He(n,p)^{3}H reaction cannot be solely attributed to the thermalization processes in the simulations. The mean ratio between experimental and simulated values is found to be 1.6 for MCNP6 and 1.1 for GEANT4, excluding the outliers at $E_p = 2.2$ MeV.

On the other hand, over the entire range, the measured count rates for scattered neutrons were larger than and had greater fluctuation than expected, implying that other objects, besides the air and walls, gave rise to neutron scattering and were not properly counted in the simulations. Nevertheless, the GEANT4 simulations predicted the total count rates and sensitivity reasonably well in the energy range.

5. Conclusion

The simulation results were validated with experimental data obtained using spontaneous-fission neutron of ^{252}Cf and quasi mono-energetic neutrons in a limited energy range. Especially, the performances of MCNP6 and GEANT4 were quantitatively investigated with quasi mono-energetic neu-

trons in the energy region between 200 keV and 1.5 MeV. Concerning detector simulation based on the ^{3}He(n,p)^{3}H reaction, GEANT4 predicted microscopic observables more realistically than did MCNP6, and MCNP6 required normalization with respect to experimental values. The results imply that GEANT4 can be a better detector simulator involving heavy-ion generations by nuclear reactions than MCNP6, while both simulation tools can equivalently estimate macroscopic observables like neutron flux. The tools can be complementarily used for neutron transport calculations depending on the type of problems to be solved; careful interpretation accompanying experimental validations may be required.

Acknowledgment This work was supported through KOMAC (Korea Multi-purpose Accelerator Complex) operation fund (KAERI-524320-23) of KAERI and by National Research Foundation of Korea (NRF) grant (No. NRF-2021R1C1C1007100) funded by the Ministry of Science and ICT (MSIT).

*pilsoolee@kaeri.re.kr

1) V. Lacoste and V. Gressier, Radiat. Meas. **45**, 1254 (2010).
2) Y. Li, T. Li, Y. Wang, B. Hong, and F. Wang, Radiat. Meas. **148**, 106662 (2021).
3) N. J. Roberts, D. J. Thomas, V. Lacoste, R. Böttger, and S. Loeb, Radiat. Meas. **45**, 1151 (2010).
4) G.-D. Kim, H.-J. Woo, J.-H. Park, Y. Tanimura, and M. Yoshizawa, J. Korean Phys. Soc. **61**, 347 (2012).
5) A. O. Hanson and J. L. McKibben, Phys. Rev. **72**, 673 (1947).
6) C. J. Werner, J. S. Bull, C. J. Solomon, F. B. Brown, G. W. McKinney, M. E. Rising, D. A. Dixon, R. L. Martz, H. G. Hughes, L. J. Cox, A. J. Zukaitis, J. C. Armstrong, R. A. Forster, and L. Casswell, Los Alamos National Laboratory (2018).
7) S. Agostinelli, J. Allison, K. Amako, J. Apostolakis, H. Araujo, P. Arce, M. Asai, D. Axen, S. Banerjee, G. Barrand, F. Behner, L. Bellagamba, J. Boudreau, L. Broglia, A. Runengo, H. Burkhardt, S. Chauvie, J. Chuma, R. Chytracek, G. Cooperman, G. Cosmo, P. Degtyarenko, A. Dell'Acqua, G. Depaola, D. Dietrich, R. Enami, A. Feliciello, C. Ferguson, H. Fesefeldt, G. Folger, F. Foppiano, A. Forti, S. Garelli, S. Giani, R. Giannitrapani, D. Gibin, J. J. Gomez Cadenas, I. Gonzalez, G. Gracia Abril, G. Greeniaus, W. Greiner, V. Grichine, A. Grossheim, S. Guatelli, P. Gumplinger, R. Hamatsu, K. Hashimoto, H. Hasui, A. Heikkinen, A. Howard, V. Ivanchenko, A. Johnson, F. W. Jones, J. Kallenbach, N. Kanaya, M. Kawabata, Y. Kawabata, M. Kawaguti, S. Kelner, P. Kent, A. Kimura, T. Kodama, R. Kokoulin, M. Kossov, H. Kurashige, E. Lamanna, T. Lampen, V. Lara, V. Lefebure, F. Lei, M. Liendl, W. Lockman, F. Longo, S. Magni, M. Maire, E. Medernach, K. Minamimoto, P. Mora de Freitas, Y. Morita, K. Murakami, M. Nagamatsu, R. Nartallo, P. Nieminen, T. Nishimura, K. Ohtsubo, M. Okamura, S. O'Neale, Y. Oohata, K. Paech, J. Perl, A. Pfeiffer, M. G. Pia, F. Ranjard, A. Rybin, S. Sadilov, E. Di Savo, G. Santin, T. Sasaki, N. Savvas, Y. Sawada, S. Scherer, S. Sei, V. Sirotenko, D. Smith, N. Starkov, H. Stoecker, J. Sulkimo, M. Takahata, S. Tanaka, E. Tcherniaev, E. Safai Tehrani, M. Tropeano, P. Truscott, H. Uno, L. Urban, P. Urban, M. Verderi, A. Walkden, W. Wander, H. Weber, J. P. Wellisch, T. Wenaus, D. C. Williams, D. Wright, T. Yamada, H. Yoshida, and D. Zschiesche, Nucl. Instrum. Methods Phys. Res., Sect. A **506**, 250 (2003).
8) J. Allison, K. Amako, J. Apostolakis, H. Araujo, P. Arce Dubois, M. Asai, G. Barrand, R. Capra, S. Chauvie, R. Chytracek, G. A. P. Cirrone, G. Cooperman, G. Cosmo, G. Cuttone, G. G. Daquino, M. Donszelmann, M. Dressel, G. Folger, F. Foppiano, J. Generowicz, V. Grichine, S. Guatelli, P. Gumplinger, A. Heikkinen, I. Hrivnacova, A. Howard, S. Incerti, V. Ivanchenko, T. Johnson, F. Jones, T. Koi, R. Kokoulin, M. Kossov, H. Kurashige, V. Lara, S. Larsson, F. Lei, O. Link, F. Longo, M. Maire, A. Mantero, B. Mascialino, I. McLaren, P. Mendez Lorenzo, K. Minamimoto, K. Murakami, P. Nieminen, L. Pandola, S. Parlati, L. Peralta, J. Perl, A. Pfeiffer, M. G. Pia, A. Ribon, P. Rodrigues, G. Russo, S. Sadilov, G. Santin, T. Sasaki, D. Smith, N. Starkov, S. Tanaka, E. Tcherniaev, B. Tome, A. Trindade, P. Truscott, L. Urban, M. Verderi, A. Walkden, J. P. Wellisch, D. C. Williams, D. Wright, and H. Yoshida, IEEE Trans. Nucl. Sci. **53**, 270 (2006).
9) J. Allison, K. Amako, J. Apostolakis, P. Acre, M. Asai, T. Aso, E. Bagli, A. Bagulya, S. Banerjee, G. Barrand, B. R. Beck, A. G. Bogdanov, D. Brandt, J. M. C. Brown, H. Burkhardt, Ph. Canal, D. Cano-Ott, S. Chauvie, K. Cho, G. A. P. Cirrone, G. Cooperman, M. A. Cortes-Giraldo, G. Cosmo, G. Cuttone, G. Depaola, L. Desorgher, X. Dong, A. Dotti, V. D. Elvira, G. Folger, Z. Francis, A. Galonyan, L. Garnier, M. Gayer, K. L. Genser, V. M. Grichine, S. Guatelli, P. Gueye, P. Gumplinger, A. S. Howard, I. Hrivnacova, S. Hwang, S. Incerti, A. Ivanchenko, V. N. Ivanchenko, F. W. Jones, S. Y. Jun, P. Kaitaniemi, N. Karakatsanis, M. Karamitros, M. Kelsey, A. Kimura, T. Koi, H. Kurashige, A. Lechner, S. B. Lee, F. Longo, M. Maire, D. Mancusi, A. Mantero, E. Mendoza, B. Morgan, K. Murakami, T. Nikitina, L. Pandola, P. Paprocki, J. Perl, I. Petrovic, M. G. Pia, W. Pokoski, J. M. Quesada, M. Raine, M. A. Reis, A. Ribon, A. RisticFira, F. Romano, G. Russo, G. Santin, T. Sasaki, D. Sawkey, J. I. Shin, I. I. Strakovski, A. Taborda, S. Tanaka, B. Rome, T. Toshito, H. N. Tran, P. R. Truscott, L. Urban, V. Uzhinsky, J. M. Verbeke, M. Verderi, B. L. Wendt, H. Wenzel, D. H. Wright, D. M. Wright, T. Yamashita, J. Yarba, and H. Yoshida, Nucl. Instrum. Methods Phys. Res., Sect. A **835**, 186 (2016).
10) Y. Wu, Fusion Sci. Technol. **74**, 321 (2018).
11) Y. Wu, J. Song, H. Zheng, G. Sun, L. Hao, P. Long, L. Hu, and FDS Team, Ann. Nucl. Energy **82**, 161 (2015).
12) C. M. Poole, I. Cornelius, J. V. Trapp, and C. M. Langton, Aust. Phys. Eng. Sci. Med. **35**, 329 (2012).
13) R. J. McConn, Jr., C. J. Gesh, R. T. Pagh, R. A. Rucker, and R. G. Williams, III, Tech. Rep. PNNL-15870 (2011).
14) ISO, ISO8529-2:2000, p. 13.
15) M. B. Chadwick, M. Herman, P. Oblozinsky, M. E. Dunn, Y. Danon, A. C. Kahler, D. L. Smith, B. Pritychenko, G. Arbanas, R. Arcilla, R. Brewer, D. A. Brown, R. Capote, A. D. Carlson, Y. S. Cho, H. Derrien, K. Guber, G. M. Hale, S. Hoblit, S. Holoway, T. D. Johnson, T. Kawano, B. C. Kiedrowski, H. Kim, S. Kunieda, N. M. Larson, L. Leal, J. P. Lestone, R. C. Little, E. A. McCutchan, R. E. MacFarlane, M. MacInnes, C. M. Mattoon, R. D. McKnight, S. F. Mughabghab, G. P. A. Nobre, G. Palmiotti, A. Palumbo, M. T. Pigni, V. G. Pronyaev, R. O. Sayer, A. A. Sonzogni, M. C. Summers, P. Talou, I. J. Thompson, A. Trkov, R. L. Vogt, S. C. van der Marck, A. Wallner, M. C. White, D. Wirada, and P. G. Young, Nucl. Data Sheets **112**, 2887 (2011).
16) The Joint Evaluated Fission and Fusion File (JEFF) 3.3, [Online]. Available: https://www.oecd-nea.org/dbdata/jeff/jeff33.
17) H. Liskien and A. Paulsen, At. Data Nucl. Data Tables **15**, 57 (1975).
18) P. Lee, J. J. Dang, H. S. Kim, H. J. Kwon, S. H. Lee, and Y. S. Cho, J. Phys.: Conf. Ser. **1350**, 012066 (2019).
19) R. Brun and F. Rademakers, Nucl. Instrum. Methods Phys. Res., Sect. A **389**, 81 (1997). See also "ROOT" [software], Release v.6.16/00, 05/02/2019, https://root.cern/content/release-61600.
20) G. F. Knoll, *Radiation Detection and Measurement* (Wiley, New York, 2010) 4th ed., p. 566.
21) H. Sekimoto and Y. Udagawa, J. Nucl. Sci. Technol. **43**, 189 (2006).